Electronic Supplementary Information

Observation of osmotically driven, highly controllable and reconfigurable oil/water phase separation

Ning Gao[a]‡, Jiecheng Cui[a]‡, Wanlin Zhang[a], Kai Feng[a], Yun Liang[a], Shiqiang Wang[a], Peng Wang[a], Kang Zhou[a], and Guangtao Li[a]*

[a]Department of Chemistry, Key Lab of Organic Optoelectronics and Molecular Engineering, Tsinghua University, Beijing 100084, P. R. China

‡Co-first authors: Ning Gao; Jiecheng Cui

*Corresponding authors:
Prof. Dr. Guangtao Li (lgt@mail.tsinghua.edu.cn)

1. General

Commercially available reagents and solvents were used as purchased from the chemical suppliers without further purification. 1-vinylimidazole, 1-bromopropane, 1-bromobutane, 1-bromohexane, 1-bromooctane, 1-bromodecane, bis(trifluoromethane)sulfonimide lithium, poly(vinyl alcohol) Mw=13000-23000 with 98% hydrolyzed, 3,4-ethoxylene dioxy thiophene, vitamin C, tetraethyl orthosilicate and dopamine were purchased from Sigma-Aldrich. ^{1}H NMR spectra were recorded on a 400 MHz NMR spectrometer (JEOL, ECS-400). The optical images of spheres were taken using an inverted fluorescence microscope (OLYMPUS, IX71) equipped with a CCD camera (OLYMPUS, DP73). The porous microspheres were characterized using scanning electron microscope (SEM) (Hitachi, SU8010). Confocal laser microscopic images were taken from Nikon N-SIM microscope. Electrochemical analysis was carried out by using HEKA PG310 potentiostat.

2. Synthesis of the polymerizable ionic liquids ($C_n$vim[Tf_2N])

1-alkyl-3-vinylimidazolium bis(trifluoromethanesulfonyl)imide ($C_n$vim[Tf_2N] n=3, 6, 8, 10) compounds were synthesized and used as polymerizable ionic liquids. The synthetic procedure was adopted according to the literature with slight modification. (*J. Mater. Chem.* ***19***, 4960-4964, 2009; *Phys. Chem. Chem. Phys.*, **13**, 16831-16840, 2011) After the formation of 1-alkyl-3-vinylimidazolium bromide ($C_n$vim[Br]) the ionic liquids with Br^- as counter-ion were converted into $C_n$vim[Tf_2N] by adding $LiTf_2N$ salt into aqueous solution of $C_n$vim[Br]. The formed $C_n$vim[Tf_2N] oils were washed with distilled water for 3 times and treated by vacuum drying for 20 hours at 70 °C to get the pure products.

^{1}H NMR (C_3vim[Tf_2N], 400 MHz, DMSO): δ 9.52 (1H, s), 8.21 (1H, s), 7.94 (1H, s), 7.30 (1H, dd, J = 8.8 Hz, J = 15.6 Hz), 5.96 (1H, dd, J = 2.3 Hz, J = 15.7 Hz), 5.43 (1H, dd, J = 2.3 Hz, J = 8.7 Hz), 4.17 (2H, t, J = 7.1 Hz), 1.91-1.79 (2H, m), 0.88 (3H, t, J = 7.4 Hz). ^{13}C NMR(C_3vim[Tf_2N], 400 MHz, DMSO): δ 135.83, 129.38, 123.73, 121.09, 119.70, 118.95, 109.10, 51.27, 23.07, 10.82. MS: calcd. For C_3vim^+(m/z)$^+$: 137; found: 137.107.

^{1}H NMR (C_6vim[Tf_2N], 400 MHz, DMSO): δ 9.48 (1H, s), 8.20 (1H, s), 7.94 (1H, s), 7.30 (1H, dd, J = 8.8 Hz, J = 15.6 Hz), 5.97 (1H, dd, J = 2.3 Hz, J = 15.7 Hz), 5.42 (1H, dd, J = 2.3 Hz, J = 8.7 Hz), 4.19 (2H, t, J = 7.1 Hz), (2H, m), 1.86-1.79 (2H, m), 1.32-1.23 (6H, m), 0.88 (3H, t, J = 7.4 Hz). ^{13}C NMR(C_6vim[Tf_2N], 400 MHz, DMSO): δ 135.79, 129.34, 123.70, 121.61, 119.64, 118.41, 108.99, 49.76, 31.03, 29.55, 25.65, 22.32, 14,15. MS: calcd. For C_6vim^+(m/z)$^+$: 179; found: 179.153.

^{1}H NMR (C_8vim[Tf_2N], 400 MHz, $CDCl_3$): δ 9.03 (1H, s), 7.67 (1H, s), 7.46 (1H, s), 7.14 (1H, dd, J = 8.8 Hz, J = 15.6 Hz), 5.81 (1H, dd, J = 2.3 Hz, J = 15.7 Hz), 5,44 (1H, dd, J = 2.3 Hz, J = 8.7 Hz), 4.24 (2H, t, J = 7.1 Hz), 1.95-1.79 (2H, m), 1.28-1.35 (10H, m), 0.89 (3H, t, J = 7.4 Hz). ^{13}C NMR(C_8vim[Tf_2N], 400 MHz, DMSO): δ 135.80, 129.36, 123.72, 121.10, 119.67, 118.96, 109.03, 49.79, 31.65, 29.60, 28.94, 28.83, 26.01, 22.53, 14.27. MS: calcd. For C_8vim^+(m/z)$^+$: 207; found: 207.184.

^{1}H NMR (C_{10}vim[Tf_2N], 400 MHz, DMSO): δ 9.46 (1H, s), 8.19 (1H, s), 7.92 (1H, s), 7.27 (1H, dd, J = 8.8 Hz, J = 15.6 Hz), 5.93 (1H, dd, J = 2.3 Hz, J = 15.7 Hz), 5.41 (1H, dd, J = 2.3 Hz, J =

8.7 Hz), 4.20 (2H, t, J = 7.1 Hz), 1.85-1.75 (2H, m), 1.38-1.16 (14H, m), 0.84 (3H, t, J = 7.4 Hz). ^{13}C NMR(C_3vim[Tf_2N], 400 MHz, DMSO): δ 135.80, 129.36, 123.72, 121.10, 119.67, 118.97, 109.02, 49.79, 31.79, 29.64, 29.39, 29.30, 29.17, 28.87, 26.01, 22.58, 14.29. MS: calcd. For C_{10}vim$^+$(m/z)$^+$: 235; found: 235.215.

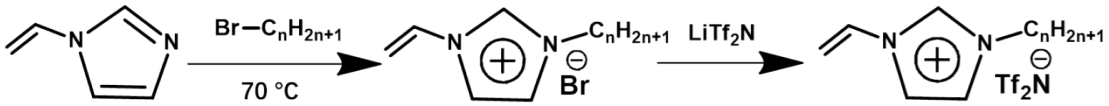

Fig. S1 Synthetic routes to imidazolium-based ionic liquids.

3. Co-flow capillary microfluidic device

Large amount of $LiTf_2N$ salt can be easily dissolved in the synthesized ionic liquids ($C_n$vim[Tf_2N]) to form homogenous oil solutions ($C_n$vim[Tf_2N]-$LiTf_2N$). Thus, a series of solutions with different molar ratios was prepared and used as special oil systems for studying their osmotically driven phase separation behaviour. A co-flow capillary microfluidic device was employed to study the phase separation process of the oil droplet in water, as shown in Figure S2. To arrest the thermodynamic metastable structures during the phase separation process, 1% 2-hydroxy-2-methylpropiophenone (w/w) as photoinitiator was added into the disperse $C_n$vim[Tf_2N]-$LiTf_2N$ oil phase for initiating the polymerization of $C_n$vim[Tf_2N] under UV light. The continuous phase was water containing 10% low Mw PVA (w/w) for stabilizing oil droplets. In our case, when the generated oil droplets were contacted with continuous water phase at the orifice of the channel the phase separation took place.

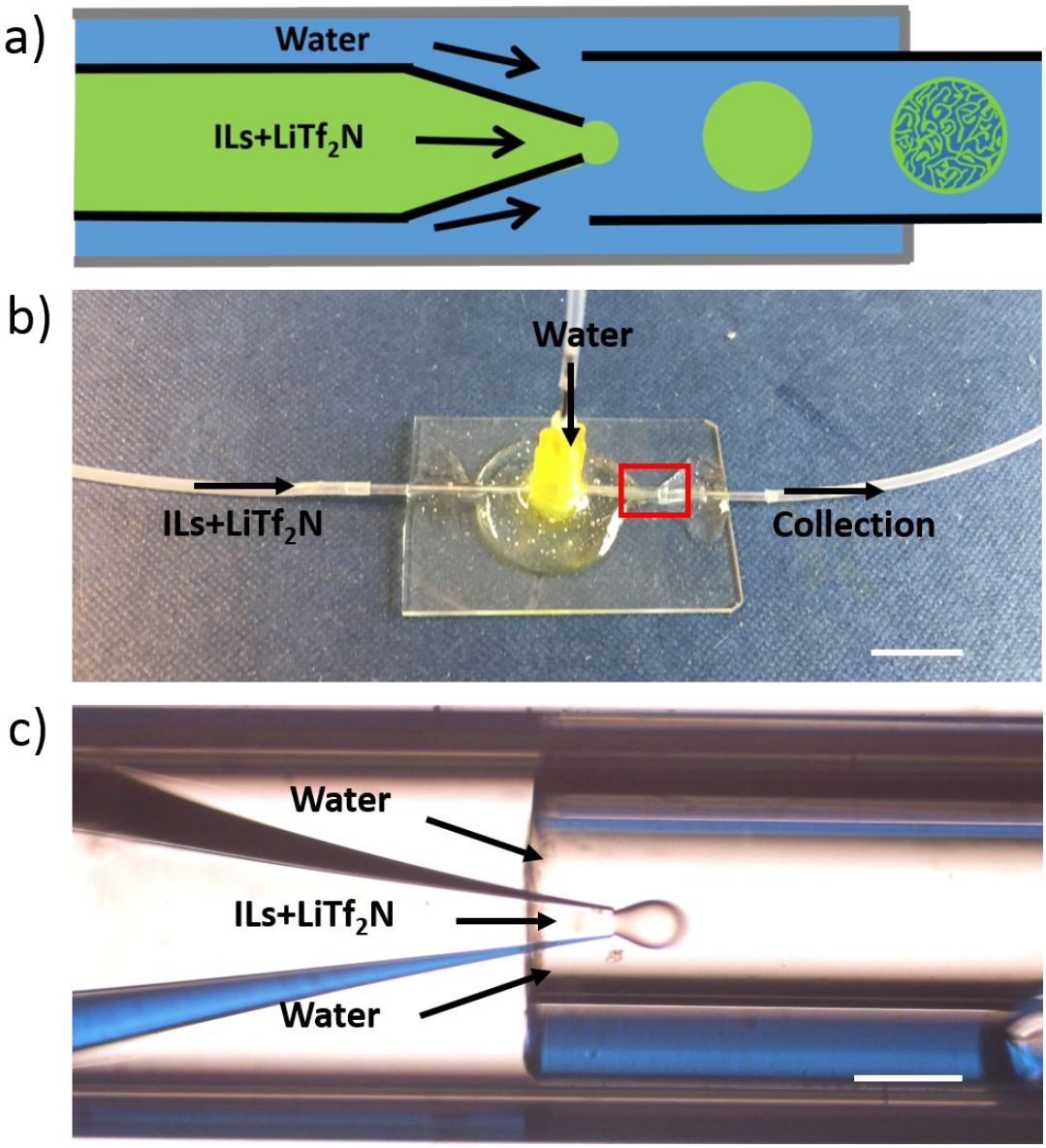

Fig. S2 (a) Schematic image of co-flow capillary microfluidic device used in this work. The continuous phase was 10% low Mw PVA (w/w) aqueous solution. The disperse phase was mixture of ionic liquid, $LiTf_2N$ salt and photoinitiator. The flow speed of continuous phase was 5-10 ml/h. The flow speed of disperse phase was 0.1-0.3 ml/h. (b) Photograph of co-flow microfluidic system. The water and oil phases are injected by plastic tubes which connected to syringe pumps. (c) Microscope image of the co-flow microfluidic chip which is marked red rectangle in (b). Scale bar are 1 cm (b) and 200 μm (c).

4. Evolution of microdroplet from transparent to cloudy appearance.

Figure S3 shows the evolution of ionic liquid/salt microdroplet after injection into aqueous solution. Firstly, the microdroplet was transparent (Fig. S3a). After adsorption of water, the microdroplet slowly turned to cloudy appearance because of the refractive index mismatch between water and ionic liquid (Fig. S3b-c).

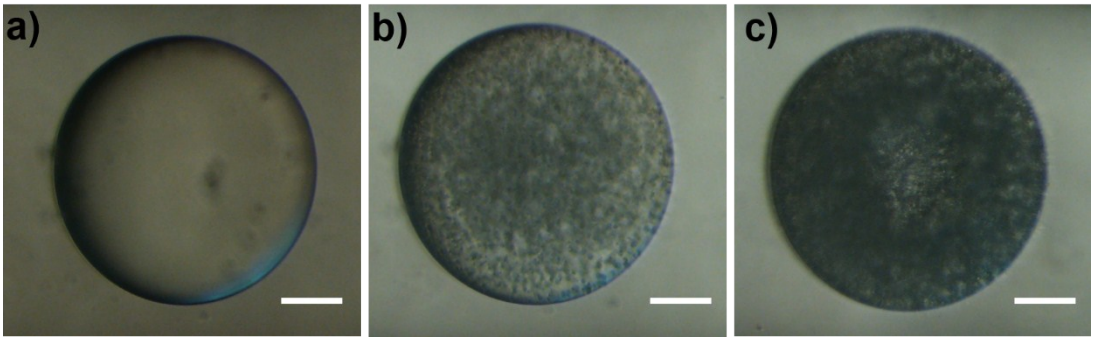

Fig. S3 Optical images of microdroplet evolution before (a) and after (b-c) adsorption of water. These pictures were taken by using transmission microscope. Scale bar is 100 μm.

5. Ternary phase diagram of water-LiTf$_2$N-C$_3$vim[Tf$_2$N] system

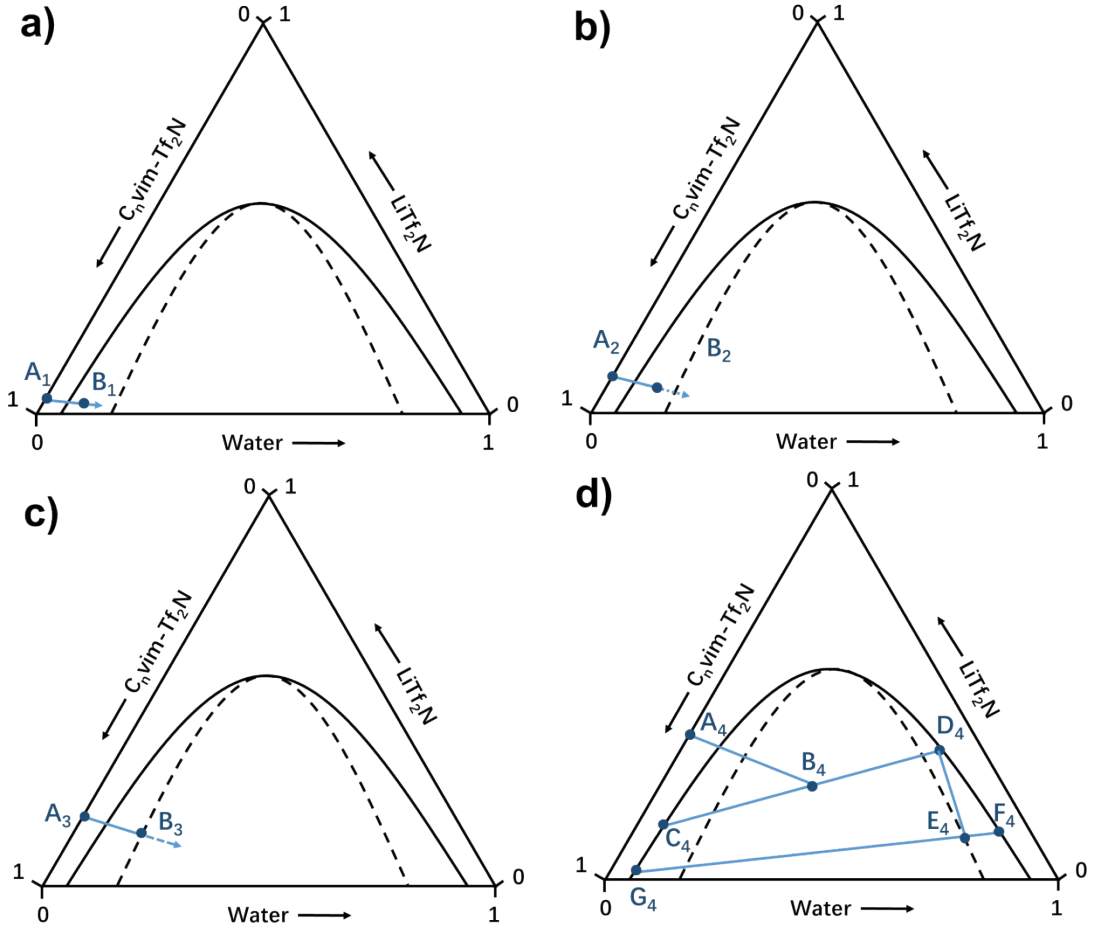

Fig. S4 Hypothetical ternary phase diagram and phase separation process by using different molar ratio of C$_3$vim[Tf$_2$N]-LiTf$_2$N mixture. The molar ratio of C$_3$vim[Tf$_2$N]-LiTf$_2$N are 40:1(a); 10:1(b); 5:1(c) and 2:1(d).

C$_3$vim[Tf$_2$N]-LiTf$_2$N-water hypothetical ternary phase diagrams were shown in Fig. S4. As shown in figure S4a, the original microdroplet contained 40:1 C$_3$vim[Tf$_2$N]-LiTf$_2$N mixture (Point A$_1$, homogeneous phase). Since the osmotic pressure of the microdroplet exceeded the Laplace pressure, water was adsorbed into the microdroplet in a slow fashion. The water flow induced the composition change. As a consequence, the composition of microdroplet passed into binodal region

(Point B_1, sea-island phase). After that, small aqueous droplets started to form inside the microdroplet.

When we increased the concentration of $LiTf_2N$, the original microdroplet was 10:1 $C_3vim[Tf_2N]$-$LiTf_2N$ mixture (Point A_2, homogeneous phase). Since the osmotic pressure of the microdroplet far exceeded the Laplace pressure, water was quickly adsorbed into the microdroplet. The water transfer induced the composition change. As a consequence, the composition of microdroplet passed into spinodal region (Point B_2, bicontinuous phase). After that, small aqueous droplets started to form inside the microdroplet. These small aqueous droplets were not stable and much of it coalesced with each other. Finally, the microdroplet turned to a core-shell structure with emulsified ionic liquid shell and big aqueous core.

Phase separation process of 5:1 $C_3vim[Tf_2N]$-$LiTf_2N$ mixture was depicted in figure S4c. 5:1 $C_3vim[Tf_2N]$-$LiTf_2N$ mixture show similar phase separation behavior with 10:1 $C_3vim[Tf_2N]$-$LiTf_2N$ mixture except the faster water adsorption.

Multiple emulsions with onion-like structure could be prepared by using 2:1 $C_3vim[Tf_2N]$-$LiTf_2N$ mixture to process osmotically driven phase separation. As shown in Fig. S6d, $C_3vim[Tf_2N]$-$LiTf_2N$-water hypothetical ternary phase diagram describes the phase separation process. The original microdroplet contained 2:1 $C_3vim[Tf_2N]$-$LiTf_2N$ mixture (Point A_4, homogeneous phase). Since the osmotic pressure of the microdroplet far exceed the Laplace pressure, water was adsorbed into the microdroplet in a fast speed. The composition of microdroplet quickly came to spinodal region (Point B_4), following by spinodal decomposition to get ionic liquid rich phase (Point C_4) and water rich phase (Point D_4). Steadily adsorption of water leads to decomposition of the inner water-rich phase. As a consequence, the inner water-rich phase separated into another water-rich phase (Point F_4) and ionic liquid rich phase (Point G_4).

6. Pure $C_3vim[Tf_2N]$ droplet in aqueous phase

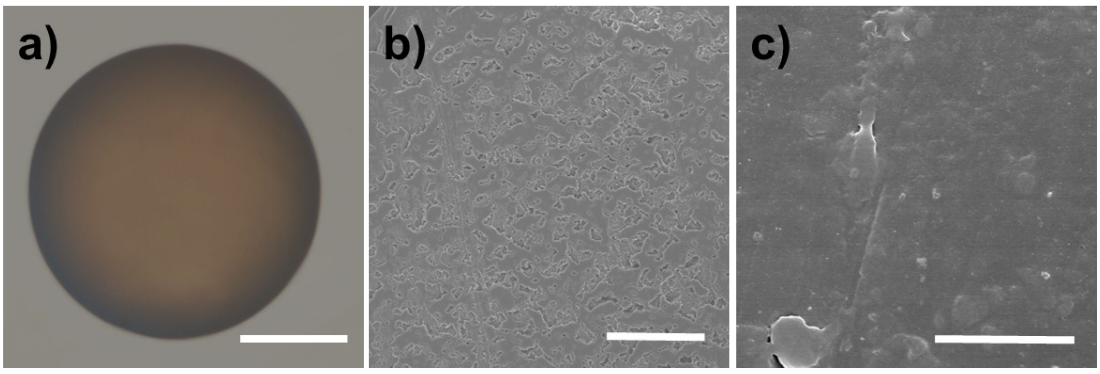

Fig. S5 (a) Optical image of pure $C_3vim[Tf_2N]$ dispersed in 10% PVA aqueous solution for ca. 60 min. SEM images of outer shell (b) and inner core (c) structure of polymerized $C_3vim[Tf_2N]$ droplet in (a). The wrinkles in (b) derived from the interfacial instability of ionic liquid-water interface. Scale bar are 100 μm for optical images (a) and 20 μm for SEM images (b, c).

7. Self-similar behavior of multiple emulsions prepared at a molar ratio of 2:1

Multiple emulsions could be prepared by using 2:1 $C_3vim[Tf_2N]$-$LiTf_2N$ mixture. In this respect, the diameter of the inner droplet had a linear relationship with the size of the initial microdroplets. Namely, we could modulate the inner droplet size on demand by simply changing the initial microdroplet diameter.

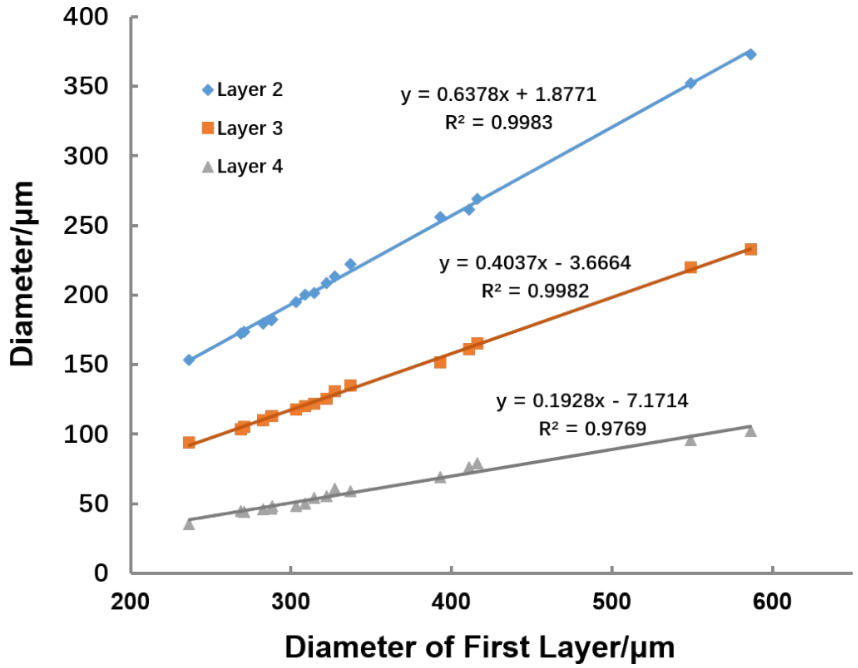

Fig. S6 Self-similar behavior of multiple emulsions prepared by 5:1 $C_3vim[Tf_2N]$-$LiTf_2N$ mixture.

8. Phase separation process by different molar ratio of $C_3vim[Tf_2N]$-$LiTf_2N$ mixture

Osmotically driven phase separation was performed by different molar ratio of $C_3vim[Tf_2N]$-$LiTf_2N$ mixture. Fig. S7 shows the bright filed images of phase separation process. As can be seen from the picture, large scale microspheres showed similar phase separation behavior, indicating the highly reproducible phase separation. When the initial molar ratio of $C_3vim[Tf_2N]$-$LiTf_2N$ was 10:1, the phase separation took place in a slow fashion. And the prepared double emulsion had a smaller inner core and thicker shell (Fig. S7a-c). As the $LiTf_2N$ concentration increased ($C_3vim[Tf_2N]$-$LiTf_2N$ = 5:1), the phase separation took place a little bit faster. At this condition, the prepared double emulsion had a bigger core and thinner ionic liquid shell (Fig. 7d-f). When we used 2:1 $C_3vim[Tf_2N]$-$LiTf_2N$ mixture, the osmotically driven phase separation took place in a violent fashion. We could get high-ordered multiple emulsions, as shown in Fig. 7g-i.

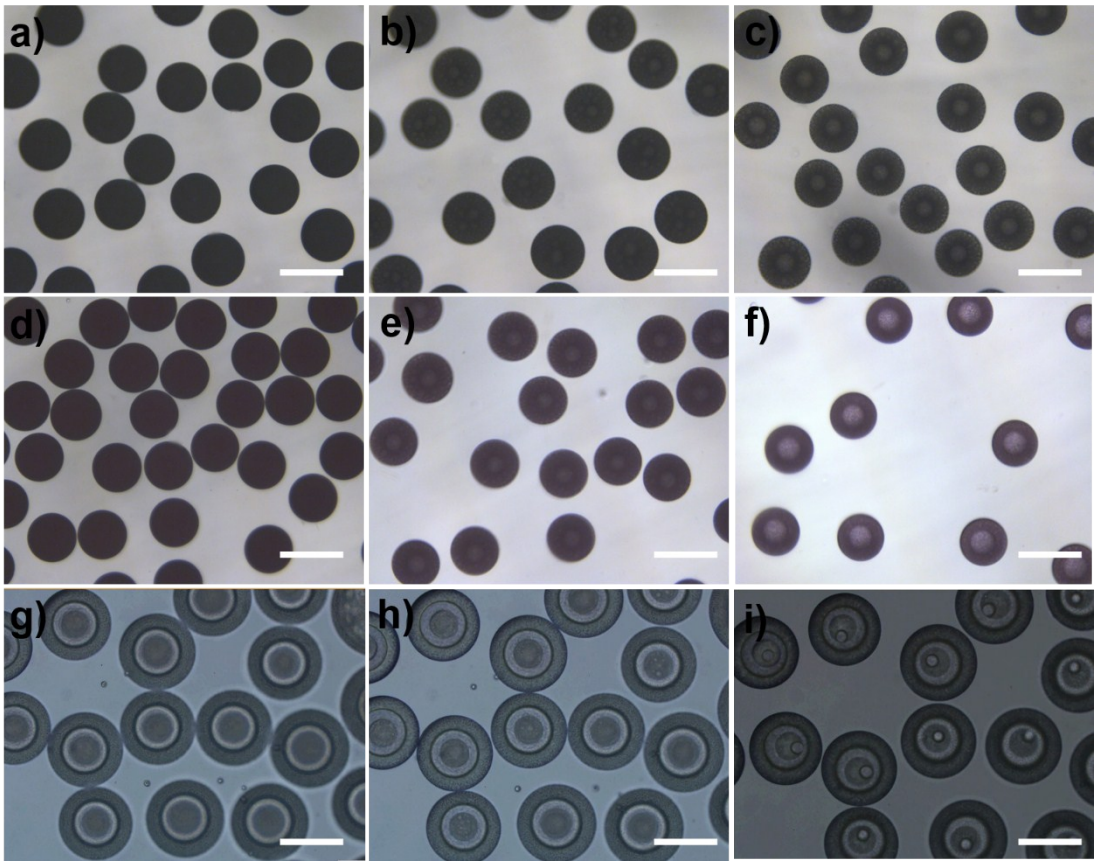

Fig. S7 Structure evolution of osmotically driven phase separation by different molar ratio of C_3vim[Tf_2N]-LiTf_2N mixture. The molar ratios were 10:1 (a-c), 5:1(d-f) and 2:1 (g-i). These pictures were taken by transmission microscope under bright field. Scale bar is Scale bar is 400 μm.

9. Double emulsions with different shell thickness.

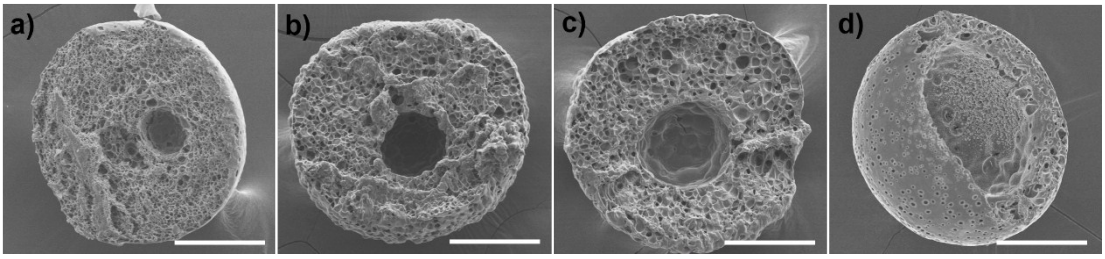

Fig. S8 SEM images of double emulsions with different shell thickness. Scale bar is 200 μm.

10. Osmotic driven phase separation by using 5:1 (mol/mol) C_8vim[Tf_2N]-LiTf_2N mixture

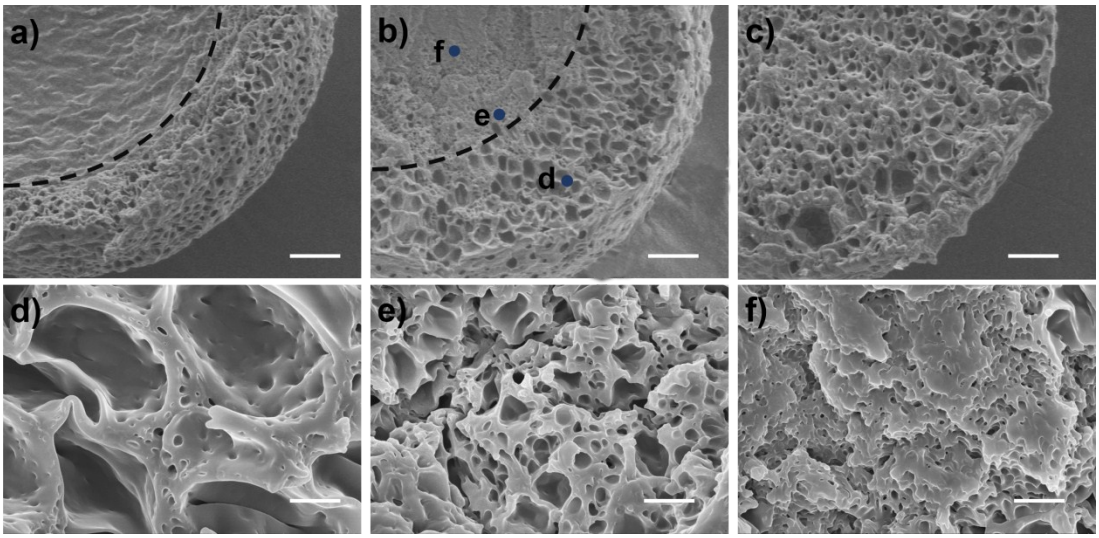

Fig. S9 SEM images of structure evolution during phase separation process by C_8vim[Tf_2N]-LiTf_2N mixture (molar ratio =5 : 1) in 2 minutes (a), 10 minutes (b), and 20minute (c). SEM photographs of the gradient porous distribution in b (d-f). Scale bar are 50μm (a-c) and 2 μm (d-f).

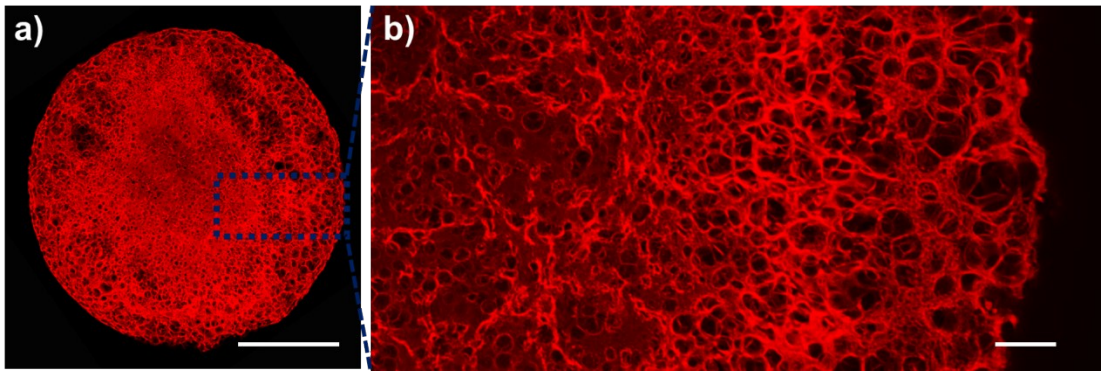

Fig. S10 CLSM images of gradient emulsion. Nile red was added into ionic liquid mixture for visualization. Scale bar are 100 μm (a) and 10 μm (b).

11. "Reconfigurable" process of osmotically driven phase separation (dehydration)

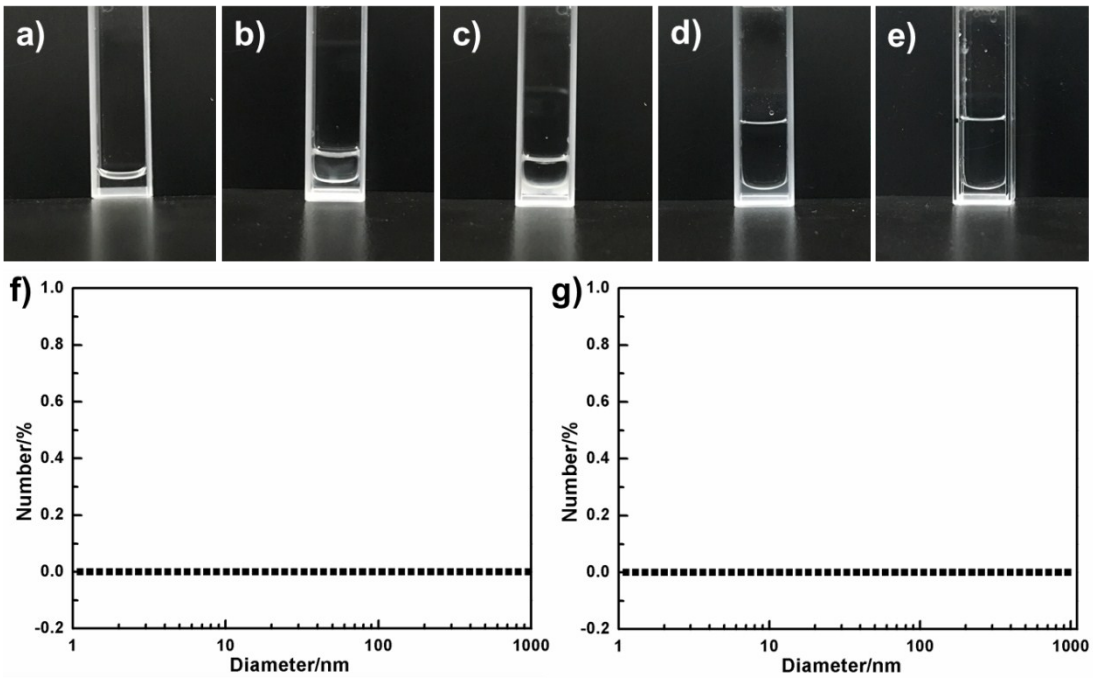

Fig. S11 Optical images of phase separation and "reconfigurable" phase separation process by using 5:1 C_6vim[Tf_2N]-LiTf_2N. (a) 5:1 C_6vim[Tf_2N]-LiTf_2N mixture; (b-c) phase separation by adding water. Water was on the top layer because of lower density; (d-e) "reconfigurable" phase separation by adding saturated NaCl aqueous solution. NaCl aqueous solution was on the top layer because of lower density. (f) DLS spectra of ionic liquid mixture in (a); (g) DLS spectra of ionic liquid mixture in (e).

12. Functional monomers

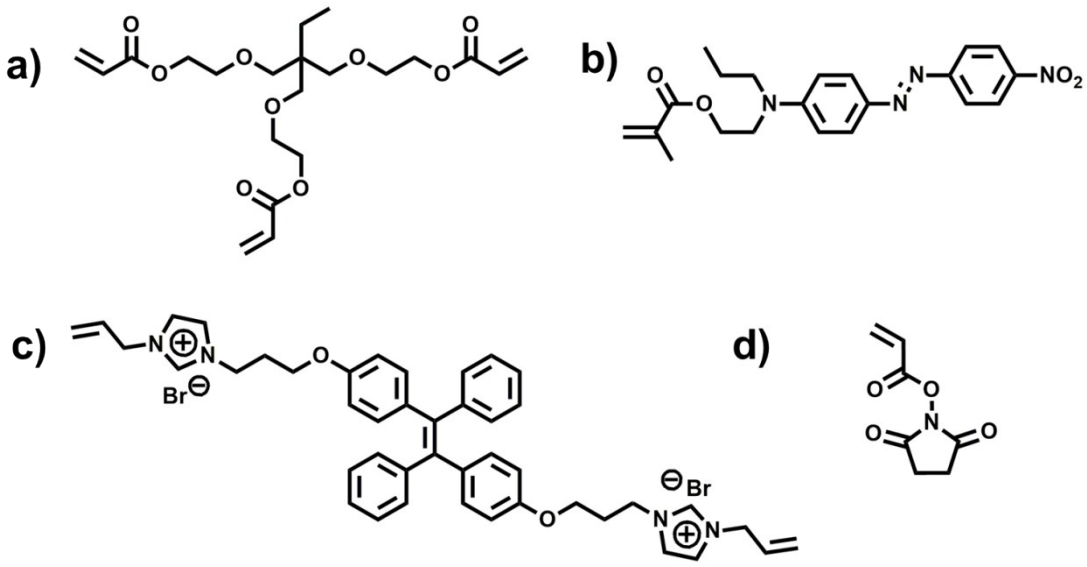

Fig. S12 Chemical structure of the functional monomers dissolved into ionic liquid mixture. (a) Ethoxylated trimethylolpropane triacrylate (ETPTA, crosslinker); (b) azobenzene-type monomer (photo-responsive materials); (c) tetraphenylethylene-type luminogen (aggregation induced emission fluorescence marker); (d) N-Acryloxysuccinimide (bioorthogonal molecular).

13. Phase separation of ionic liquid/salt/carbon nanotube mixture

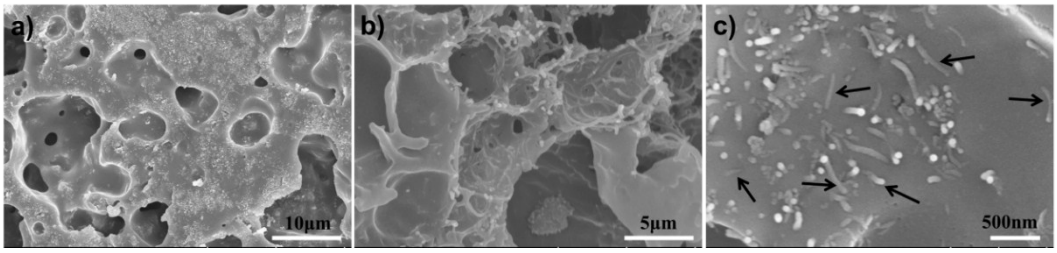

Fig. S13 SEM images of emulsion prepared by using ionic liquid/salt/carbon nanotubes mixture. Black arrows describe the pristine multiwall carbon nanotubes.

14. Phase separation of ionic liquid/salt/Au nanoparticles mixture

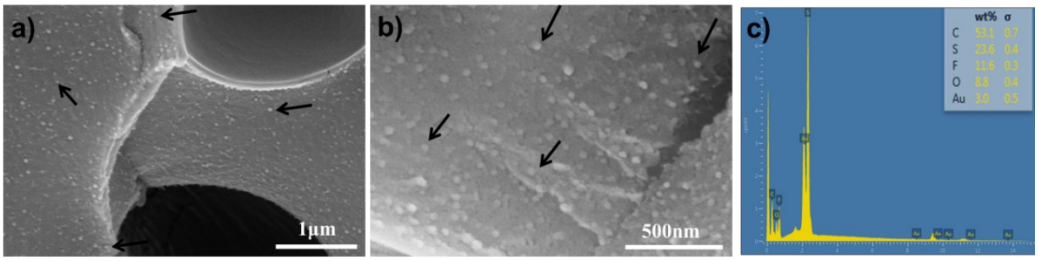

Fig. S14 (a-b) SEM images of emulsion prepared by using ionic liquid/salt/Au nanoparticles mixture. Black arrows describe the pristine Au nanoparticles. (c) Element analysis of Au nanoparticles doped emulsion.

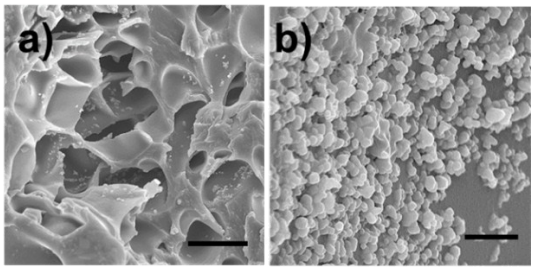

Fig. S15 (a-b) SEM images of the porous structure prepared by using ionic liquid/salt/TiO2 particles mixture. Scale bar are 10 μm (a) and 1μm (b).

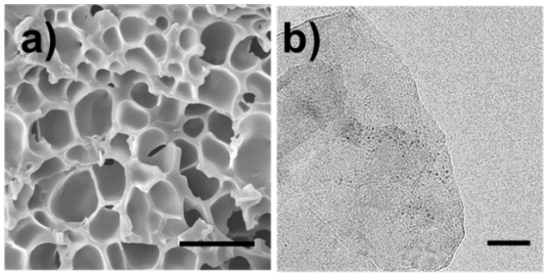

Fig. S16 SEM image (a) of the porous structure prepared by using ionic liquid/salt/graphene mixture and the corresponding TEM image (b). Scale bar are 10 μm (a) and 1μm (b).

15. Preparation of functional porous materials through OPS process

$C_n$vim[Tf_2N]-LiTf_2N system could serve as a general carrier platform to guide the phase separation of the dissolved or dispersed species and objects, affording various functional porous materials. In our work, by exploiting the excellent solvency of ionic liquids, various species or objects, including polymerizable monomer, chromophore, bioorthogonal reactive compound, carbon nanotube, graphene, gold nanoparticles, and TiO_2 nanoparticles were dissolved or dispersed in $C_n$vim[Tf_2N]-LiTf_2N oil solution, and a series of functional porous materials was fabricated through a simple OPS process. Additionally, counteranion exchange of ionic liquids provides another means to functionalize the porous structure generated by OPS. As exemplified, in our work the porous poly(ionic liquid) spheres generated were further exposed to 0.1 M KOH aqueous solution for 12 h to prepare OH^- based porous spheres. Then, these OH^- based porous spheres were reacted with dopamine for realizing the polydopamine functionalized porous materials. The similar anion exchange procedures were employed to produce other functional porous materials.

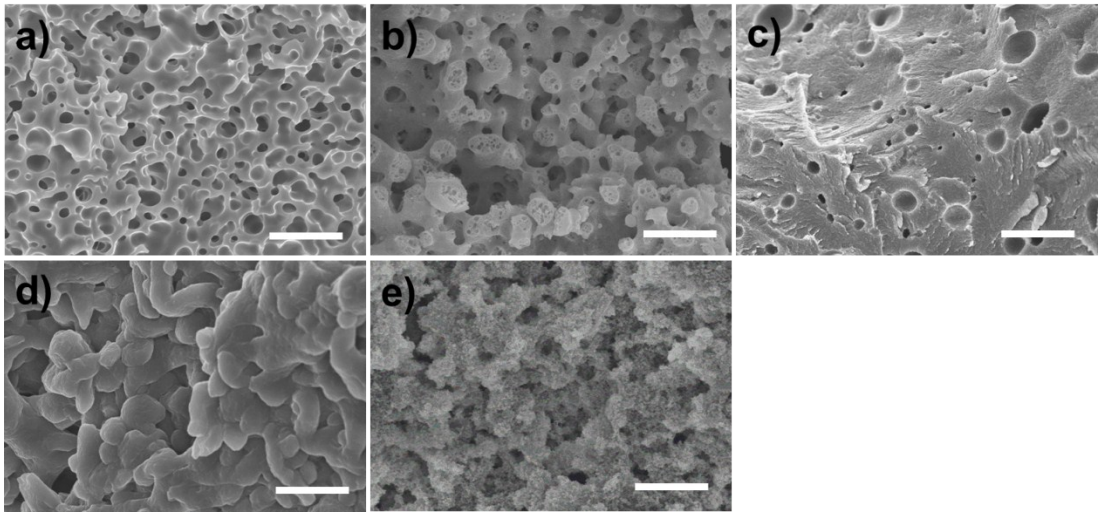

Fig. S17 SEM images of the resultant functional porous poly(ionic liquid)s by using anion exchange and subsequent reaction. (a) Tf_2N^- , (b) $HAuCl_4$, (c) Vitamin C , (d) dopamine and (e) Tetraethyl orthosilicate. Scale bar is 10 μm.

16. Preparation of bicontinuous porous films through OPS process

To demonstrate the power of OPS described here to produce functional materials, the C_8vim[Tf_2N]-LiTf_2N solution containing photoinitiator was used for the preparation of bicontinuously structured membrane that shows both ionic and electrical conductivity. Briefly, the C_8vim[Tf_2N]-LiTf_2N mixture was spin-coated onto a glass substrate. Then the coated substrate was immersed into water phase for initiating OPS process, and after polymerization under UV light the prepared film was washed with distilled water.

17. Solubility of ionic liquids in water and solubility of water in ionic liquids

With the increasement of alkyl length of ionic liquids, the solubility of water in ionic liquids decreased slightly. The solubility of $C_n$vim[Tf_2N] in water is 5-10 ul/ml (**n**=3), 1-5 ul/ml (**n**=6),

and < 1 ul/ml (**n**=8,10). On the other hand, the solubility of water in $C_n$vim[Tf_2N] are all below than 1 ul/ml (**n**=3, 6, 8, 10).

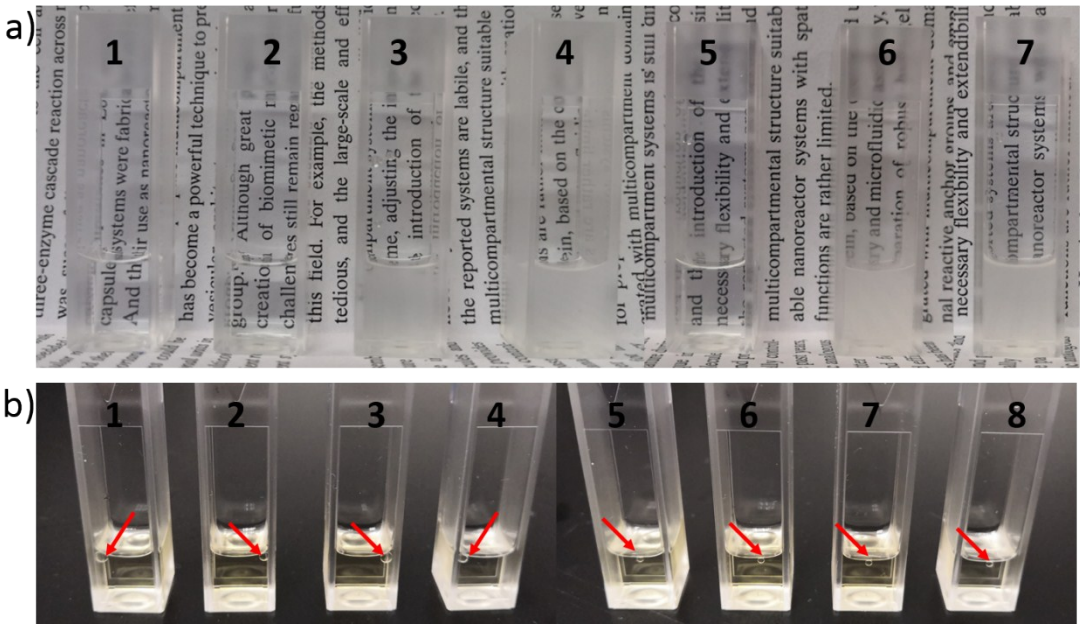

Fig. S18 (a) solubility of $C_n$vim[Tf_2N] in water: **(1)** 1 µl C_3vim[Tf_2N] in 1 ml water; **(2)** 1 µl C_6vim[Tf_2N] in 1 ml water; **(3)** 1 µl C_8vim[Tf_2N] in 1 ml water; **(4)** 1 µl C_{10}vim[Tf_2N] in 1 ml water; **(5)** 5 µl C_3vim[Tf_2N] in 1 ml water; **(6)** 5 µl C_6vim[Tf_2N] in 1 ml water; **(7)** 10 µl C_3vim[Tf_2N] in 1 ml water. (b) Solubility of water in $C_n$vim[Tf_2N]: (1) 10 µl water in C_3vim[Tf_2N]; (2) 10 µl water in C_6vim[Tf_2N]; (3) 10 µl water in C_8vim[Tf_2N]; (4) 10 µl water in C_{10}vim[Tf_2N]; (5) 1 µl water in C_3vim[Tf_2N]; (6) 1 µl water in C_6vim[Tf_2N]; (7) 1 µl water in C_8vim[Tf_2N]; (8) 1 µl water in C_{10}vim[Tf_2N]; Red arrows indicate the insoluble water droplet in the ionic liquids.

18. OPS in $C_n$vim[Tf_2N]-Li[Tf_2N] system with different Li[Tf_2N] concentration

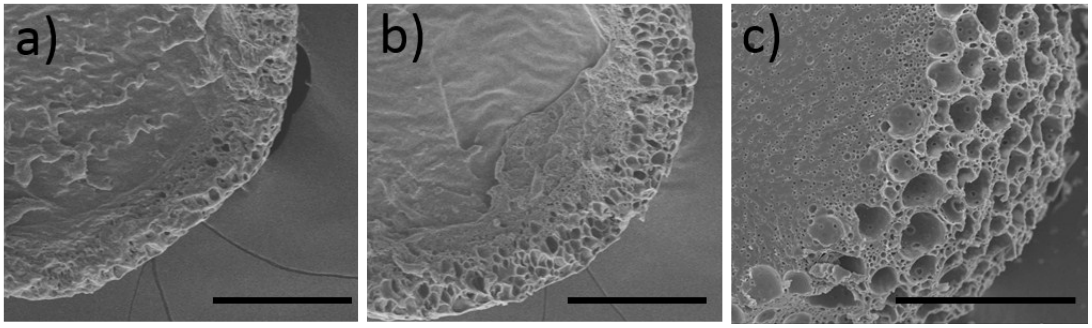

Fig. S19 (a) SEM image of polymerized emulsion after 2 minutes phase separation by using 10:1 (a), 5:1 (b) and 2:1 (c) C_8vim[Tf_2N]-LiTf_2N mixture. Scale bar is 100 µm.

19. Bicontinuous structure prepared by OPS process

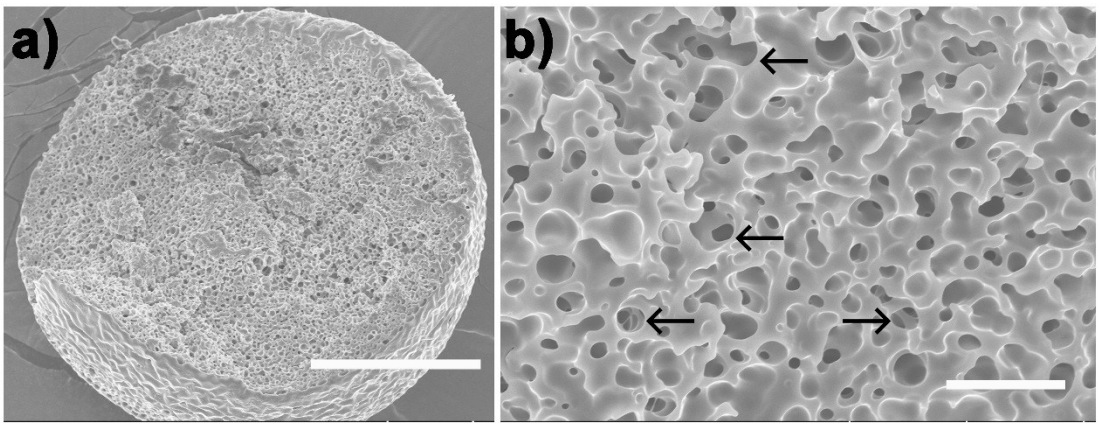

Fig. S20 SEM images of the bicontinuous structure prepared by OPS process. Black arrows in (b) show that the porous is inter-connected. Scale bar are 100 μm (a) and 10 μm (b).

20. Interfacial tension between ionic liquids and aqueous solution

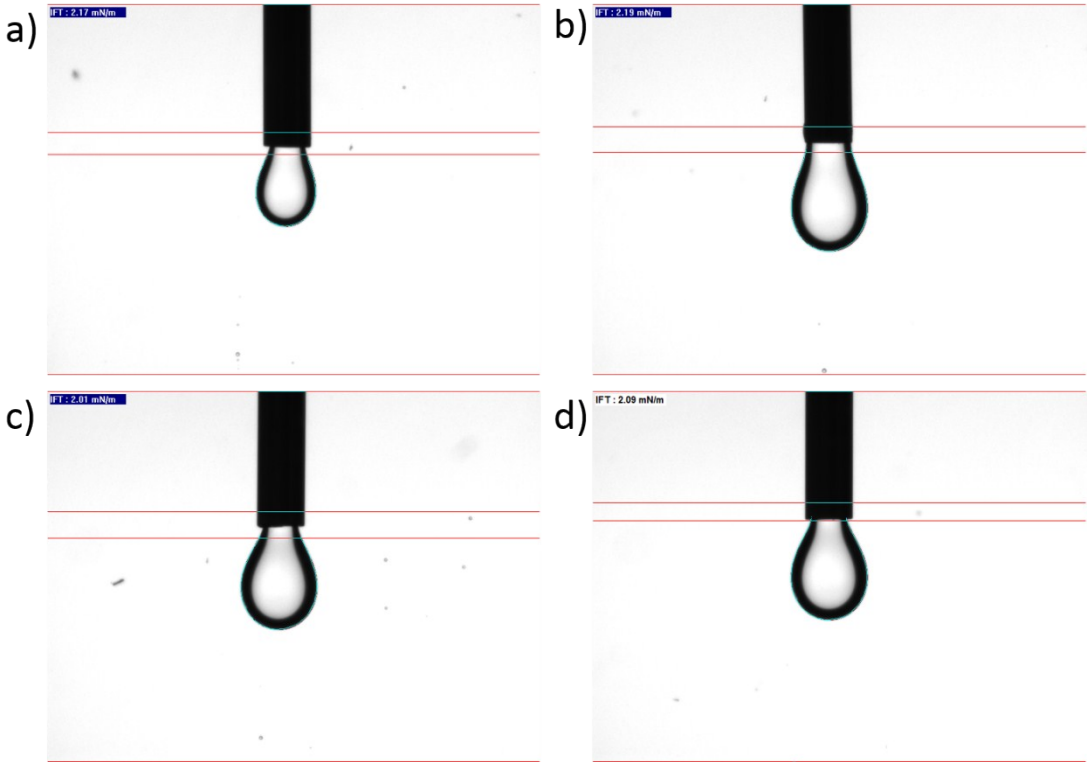

Fig. S21 Interfaical tension between $C_n$vim[Tf_2N] ionic liquids and 10% PVA aqueous solution. (a) n=3, γ=2.17 mN/m; (b) n=6, γ=2.19 mN/m; (c) n=8, γ=2.01 mN/m; (d) n=10, γ=2.09 mN/m.